J Mater Sci (2009) 44:2247–2256
DOI 10.1007/s10853-008-2962-x

FESTSCHRIFT IN HONOUR OF PROF T R ANANTHARAMAN ON THE OCCASION OF HIS 80TH BIRTHDAY

First report on observation of abnormal creep in a Zr–2.5wt.%Nb alloy at low stresses

R. Kishore · S. Banerjee · P. Rama Rao

Received: 14 May 2008 / Accepted: 20 August 2008 / Published online: 18 September 2008

Abstract Low-stress creep behaviour of a two-phase Zr–2.5%Nb alloy, differently heat treated, has been investigated using helical test specimens. The phase diagram of the α (hcp) + β (bcc) alloy is characterized by the monotectoid reaction at 893 ± 10 K: $\beta_1 \rightarrow (\alpha + \beta_2)$ where β_1 (Zr–20Nb) and β_2 (Zr–80Nb) have widely differing compositions. At the creep testing temperature, 818 K, which is close to but below the monotectoid temperature, the creep rate for samples with the equilibrium $\alpha + \beta_2$ structure has been found to be considerably higher, over an order of magnitude, than that in samples with the metastable $\alpha + \beta_1$ structure. Microstructural changes accompanying the markedly enhanced creep rate for the $\alpha + \beta_2$ structure at stresses as low as 1–4 MPa have been explained in terms of the relative stability of the β_1 and the β_2 phases during the creep process. An attempt has been made to elicit the likely mechanism underlying the observed enhancement of creep rate and the changes in morphology, composition and volume fraction of the β phase.

Introduction

The Zr–2.5 wt.%Nb alloy, used as a pressure tube material in pressurized heavy water nuclear reactors (PHWR), represents a group of $\alpha + \beta$ alloys, typical of titanium and zirconium base systems which exhibit a monotectoid reaction, $\beta_1 \rightarrow \alpha + \beta_2$, where β_1 and β_2 are bcc phases of widely differing composition and α phase is the hcp terminal solid solution [1]. The miscibility gap in the β phase field in several titanium and zirconium alloy systems, e.g. Ti–Mo, Ti–Nb, Ti–V, Zr–Nb, Zr–Ta, containing β-stabilizing alloying elements is essentially responsible for the occurrence of the monotectoid reaction in these systems. High-temperature creep data at relatively low stresses in zircaloys (zirconium base alloy with Sn, Ni, Fe and Cr as alloying additives) containing intermetallic phases Zr_2Ni and $Zr(Fe,Cr)_2$, which remain stable during high-temperature creep, are available [2, 3]. Unlike in zircaloys, the two solid solution phases, α and β, in the Zr–2.5%Nb alloy system, are expected to undergo morphological changes during high-temperature creep. The objective of the present investigation is to examine the influence of such microstructural changes on the creep behaviour of Zr–2.5wt.%Nb alloy.

R. Kishore · S. Banerjee (✉)
Bhabha Atomic Research Centre, Trombay, Mumbai 400 085, India
e-mail: sbanerji@barc.gov.in

P. Rama Rao
International Advanced Research Centre for Powder Metallurgy and New Materials (ARCI), Balapur, Hyderabad 500005, India

Experimental methods and analysis

The binary zirconium alloy used for this study contained 2.45% Nb by weight and 1500 ppm oxygen. Longitudinal strips of length 200 mm were sliced from a hot-extruded pressure tube section. These strips were machined to 6.5 mm rods and swaged at room temperature to 3.0 mm diameter with intermediate vacuum annealing at 973 K. The 3-mm rods were annealed under the same conditions for 30 min before the final reduction to 1.6 mm diameter. This treatment was necessary to prevent the hardened wire from breaking during the last pass through the final die as well as for the ease of winding the wire around a mandrel. The helical samples for creep tests were prepared by

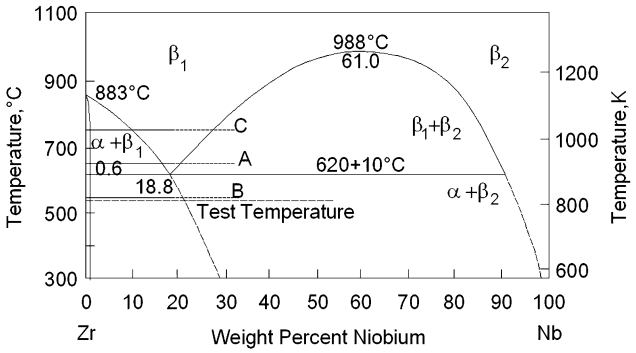

Fig. 1 Zirconium–niobium phase diagram in which are depicted the test temperature and the three heat treatment temperatures designated as A, B and C

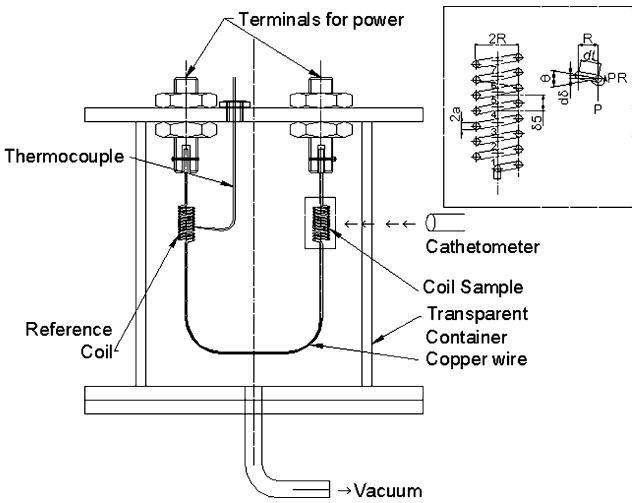

Fig. 2 Schematic of the low-stress creep apparatus used in the present study; inset shows the helical-coil sample and the various parameters used in the calculation of stress and strain in a coil

winding the wire around a 19-mm-diameter stainless steel mandrel and was then heat treated under different conditions. The results reported here pertain to three heat treatments namely, (A) soak at 923 K for 3 h and furnace cool, (B) same as in (A) followed by an ageing treatment at 823 K for 240 h and (C) soak at 1018 K for 0.75 h and furnace cool. These treatments are shown in the phase diagram (Fig. 1). Since β phase is known to be metastable and, therefore, very likely to undergo morphological and compositional changes, the treatment B involving a long period of ageing was given with the intention of stabilizing the microstructure. Accordingly, prolonged ageing was carried out at a temperature (823 K) slightly above the test temperature (818 K). The purpose of heat treatment C was to coarsen α grain size in comparison to that in A. Raising the soaking temperature to 1083 K, i.e. beyond the soaking temperature used for heat treatment C, did not result in further coarsening of α phase. The details of microstructure resulting from the three treatments are described in Table 1.

Creep experiments were conducted using helical-coil wire specimens which were rapidly heated to the test temperature by passing electric current through the specimens under vacuum better than 10^{-5} torr in a set-up similar to the one described in [4]. The creep strains in each coil due to self-load were measured as a function of time. This technique has the advantage of obtaining creep strains corresponding to different stress values from a single helical sample and is suitable for measuring very low creep strains. The set-up and the principle underlying it are schematically illustrated in Fig. 2. The heat-treated helical spring specimens were cut into two equal segments; one segment was used for actual creep measurements while the other served as a reference for temperature measurement using S-type thermocouple that was spot welded to it. Both the segments were loaded in the creep set-up by fixing the top sides of the coils to copper terminals rigidly and shorting the bottom sides by a strand of fine copper wires for electrical continuity. The coil was heated by passing stabilized and constant alternating current (AC), and the temperature was maintained within ±3 K of the set temperature throughout the experiment up to 100 h. The deflection δ, the change in the distance between two successive turns of the coil sample, was manually measured using a cathetometer having a resolution of 10 μm, which corresponds to a strain resolution of 7.25×10^{-6}.

Metallographic studies were carried out on specimens before and after creep deformation. Specimens were polished and chemically etched with a solution containing 5% HF:45% HNO_3:50% H_2O. Light microscopy was employed for grain size estimation and for characterization of phase distribution. For preparation of TEM foils, slices of wire specimens were mechanically polished and subsequently thinned using a twin-jet electro polisher maintained at a temperature of ~240 K under a voltage 25 V.

Conventional uni-axial tensile creep tests were performed on flat samples with microstructural conditions

Table 1 Microstructural features of Zr–2.5wt.%Nb alloy in helical sample

Designation	Heat treatments	Measured volume fraction of β (%)	Cross-sectional α grain size (μm)
A	923 K for 3 h furnace cool	8–10	3 ± 1.5
B	923 K for 3 h furnace cool + aged at 823 K/240 h	1.5–2	3 ± 1.5
C	1018 K/0.75 h furnace cool[a]	8–12	5.1 ± 0.5

[a] Raising annealing temperature to 1083 K did not further coarsen the α phase

corresponding to helical spring samples A and B at a stress level equal to the highest stress experienced by the coil in the helical sample. The micro-hardness data presented in Table 3 are from the flat tensile samples.

Results and discussion

Creep rate

Typical deflection–time plots obtained from the helical spring specimens A and B for a few stress levels are shown in Fig. 3. Each of the δ–t curves presented in Fig. 3 represents each coil in the spring and the deflections are shown on the Y-axis. These experimental curves are displaced in the Y direction for clarity. The scale for the Y-axis is indicated.

The rate of deflection $(\dot{\delta})$ and the load (P) on the coil are converted to tensile strain rate $\dot{\varepsilon}$ and tensile stress (σ), respectively, using the two relations [4–6] given in Eq. 1, where a and R are the radius of the wire and the coil, respectively, as illustrated in Fig. 2:

$$\sigma = \frac{2\sqrt{3}PR}{\pi a^3}; \quad \dot{\varepsilon} = \frac{a}{2\sqrt{3}\pi R^2}\dot{\delta} \tag{1}$$

The deflection of the coil (θ in Fig. 2) is kept within 10° so that the relations remain valid throughout the experiment.

The plots of creep rate vs. applied stress values (σ_a), on logarithmic scale, are shown in Fig. 4a. If the data are plotted on a linear scale, a threshold value of stress (σ_{th}) is seen below which the creep rate was too low to be measured. A typical plot for treatment B is shown in the inset. The threshold stress values thus measured for treatments A, B and C, respectively, are 1.55, 0.83 and 0.90 MPa. The threshold stress was subtracted from the applied stress to obtain the effective stress $(\sigma_{eff} = \sigma_a - \sigma_{th})$ for the corresponding treatments.

The plot of creep rate $(\dot{\varepsilon}_c)$ vs. the effective stress (σ_{eff}) for samples A–C tested at 818 K, on logarithmic scale, are shown in Fig. 4b. The measured stress exponent of unity suggests occurrence of diffusional creep in these samples.

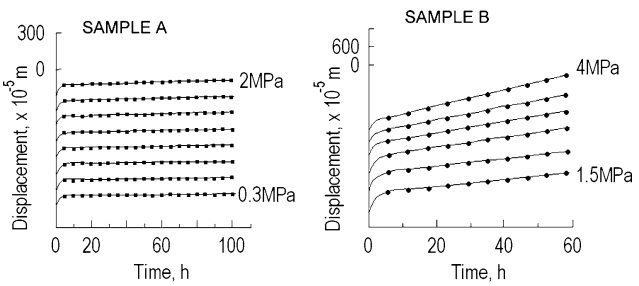

Fig. 3 Typical displacement vs. time plots for samples A and B at 818 K (helical sample)

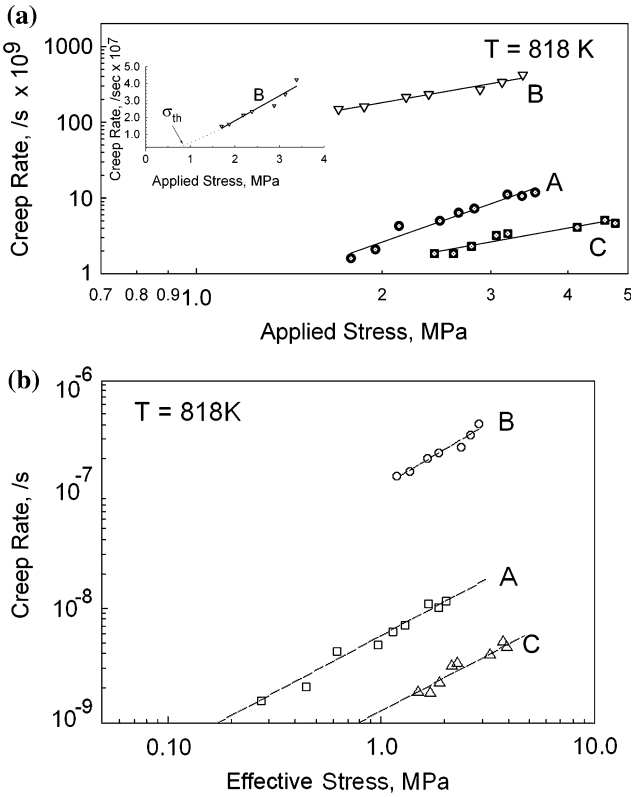

Fig. 4 Plots of (**a**) creep rate $\dot{\varepsilon}$ vs. applied stress on logarithmic scale; inset shows a typical plot for sample B on linear scale and (**b**) $\dot{\varepsilon}$ vs. effective stress at 818 K for Zr–2.5%Nb alloy samples designated as A, B and C (helical sample)

The considerably higher creep rate observed in sample B is striking. For the same applied stress, say 2.0 MPa, at 818 K, the data show that the creep rate in sample B is nearly two orders of magnitude faster than in sample A (Table 2). Recalling that the intention of heat treatment imparted to sample B was to ensure a stable microstructure during the creep duration, the observed nearly runaway creep in sample B was unexpected.

Microstructural changes during creep

The microstructures of samples A and B prior to and after creep deformation are presented in Fig. 5. The striking feature is that, after the creep tests, the volume fraction of β has decreased in sample A while it has increased in sample B. In order to confirm these observations, specimens from

Table 2 Creep rates in differently heat-treated Zr–2.5wt.%Nb alloy at 818 K for an applied stress of 2.0 MPa (helical sample)

Sample ID	Creep rate (s^{-1})
A	2.5×10^{-9}
B	1.8×10^{-7}

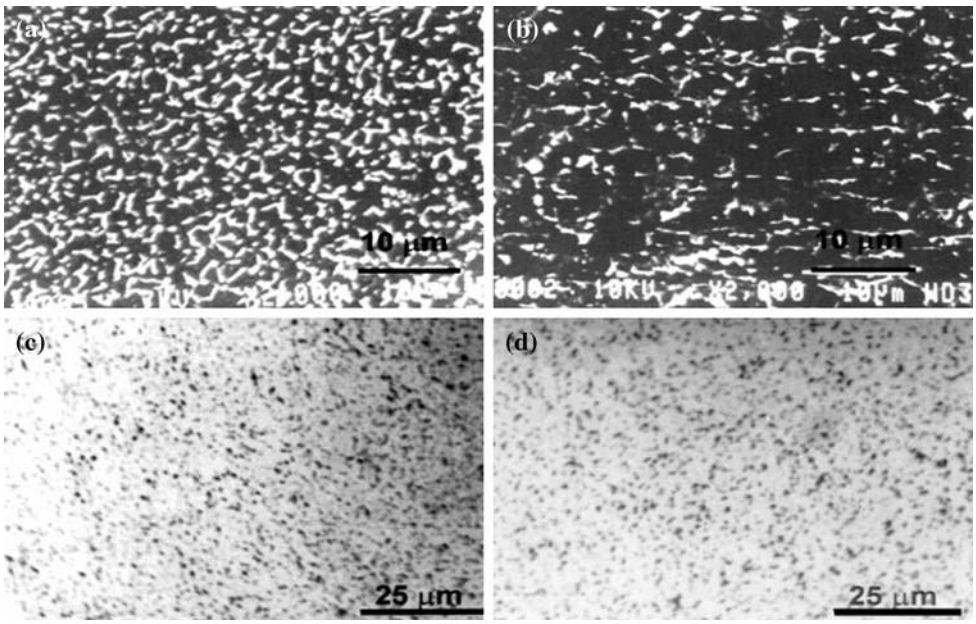

Fig. 5 Microstructure of Zr–2.5%Nb alloy before and after creep in samples A (**a** & **b**) and B (**c** & **d**) showing the change in β volume fraction (helical sample)

the same stock of Zr–2.5wt.%Nb alloys were subjected to tensile deformation at 818 K by application of load corresponding to a stress comparable to the maximum creep stress in the coil. Specimens from these tested samples were examined in the optical microscope as well as by transmission electron microscopy. The results are presented in Table 3 and Fig. 6.

Quantitative metallographic data of Table 3 validate features evident in the micrographs of Fig. 5a–d. As a result of creep, the volume fraction of β phase has diminished from about 12–14% to 9% in sample A (Fig. 5a, b) while it has increased by a factor of 2.5 in sample B from 1.6% to 4.0% (Fig. 5c, d). Micro-hardness measurements support the metallographic observations (Table 3). Since the α phase is harder than the β phase in this alloy, the measured changes in hardness correlate with the changes in the volume fraction of the α phase consequent to a decrease or increase in the β volume fraction. The transmission electron micrographs (Fig. 6) obtained from A and B materials also indicate changes in the precipitate morphology and the volume fraction of the β phase during creep.

In view of the large increase in creep rate in sample B and the observed microstructural changes during creep, microanalysis (EDS) of α and β phases was carried out. The results obtained on samples A and B are given in Table 4 and these data point to certain important features, which are listed below:

The composition of the matrix α phase has remained practically unchanged during the creep process.

The composition of the β precipitates changed from 21% to 34% Nb in sample A while it changed hugely from 80% to 30% Nb in sample B. The compositional changes in precipitates are consistent with the changes in volume fraction presented in Table 3.

It is recalled that sample B was obtained by prolonged ageing of sample A at 823 K. To start with, i.e. prior to creep, the composition of the β phase corresponded, as expected, to that of the equilibrium β_2, i.e. 80% Nb. It was surprising that after creep, the equilibrium β_2 changed composition towards that of the metastable β_1 with lower Nb content (Table 4). The question that arises is not only with respect to the cause of this change but also its role during the diffusion creep process.

The free energy-composition diagram for the Zr–2.5Nb system

The analysis of the phase diagram of the Zr–Nb system reveals a strong tendency for the β phase to undergo

Table 3 Changes in β volume fraction and in micro-hardness[a] values after creep (tensile sample)

Sample	Condition	Measured β volume fraction (wt.%)	Micro-hardness (VHN)
A	Prior to creep	12–14	164 ± 3
	After creep	9 ± 1.0	204 ± 6
B	Prior to creep	1.60 ± 0.4	247 ± 3
	After creep	4 ± 0.5	211 ± 5

[a] Micro-hardness values averaged over ten readings using a force of 9.8 N

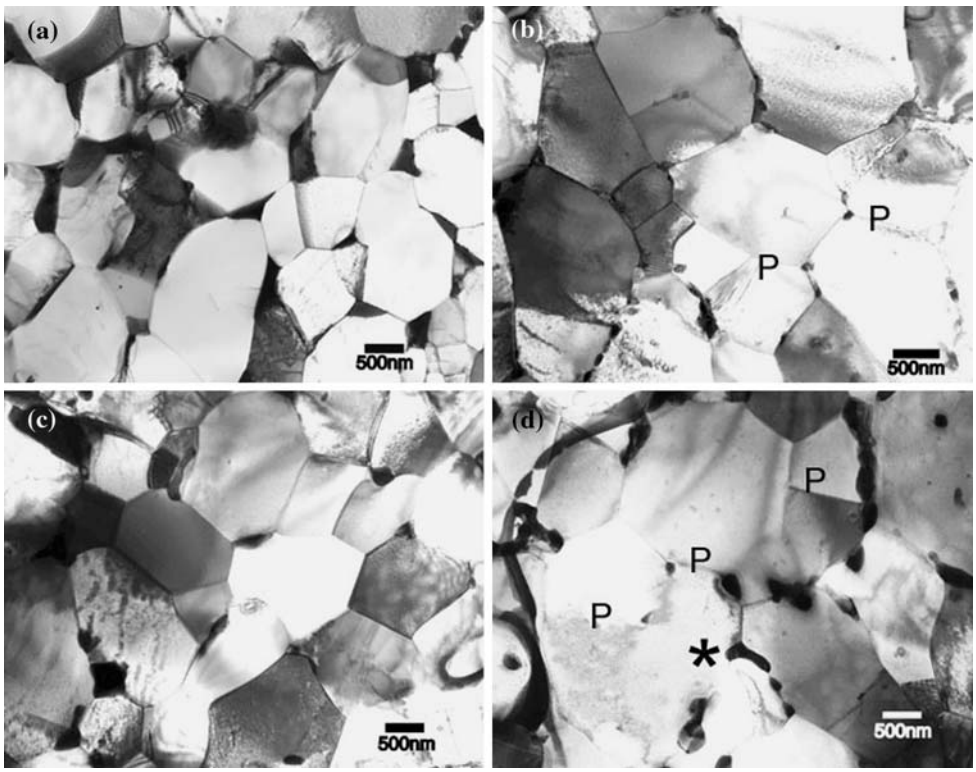

Fig. 6 TEMs of samples A (**a** & **b**) and B (**c** & **d**) showing significant changes in the β phase (dark particles) as a result of creep deformation (tensile sample)

Table 4 Microanalysis[a] (EDS) of samples A and B (tensile sample)

Sample	Phase			
	α		β	
	Before creep test	After creep test	Before creep test	After creep test
A				
Zr (wt.%)	98.4 ± 0.1	98.5 ± 0.1	79.5 ± 0.15	66.4 ± 0.5
Nb (wt.%)	1.60 ± 0.34	1.50 ± 0.50	21.3 ± 1.5	34.6 ± 5.5
B				
Zr (wt.%)	97.7 ± 0.1	98.4 ± 0.15	20.4 ± 0.1	70.1 ± 0.8
Nb (wt.%)	1.30 ± 0.25	1.40 ± 0.3	79.6 ± 1.75	29.9 ± 3.8

[a] The compositions mentioned in the table are average of measurements made on about ten β particles and at least at about ten α locations

phase separation into the Zr-rich β_1 and the Nb-rich β_2 phases [7]. The positive deviation from the ideal solid solution behaviour is reflected in the doubly inflected free energy (G) vs. concentration (c) plot for the β phase (Fig. 7). At the monotectoid temperature, 893 K, an equilibrium condition is set-up between the α, β_1 and β_2 phases as shown by the construction of the common tangents in Fig. 7. Menon et al. [7] have shown that at temperatures below, but close to the monotectoid temperature (i.e. between 783 and 893 K), a metastable equilibrium between the α and the β_1 phase controls the early stages of the precipitation of the bcc phase from the supersaturated α phase. Zr-rich side of the G–c plot (Fig. 8) shows that the free energy of the mixture of α and β_1 is only slightly higher than that of the equilibrium mixture of α and β_2 at 823 K. This can be seen from the relevant portion of the G–c diagram, which is magnified in the inset. The free energy associated with the metastable equilibrium ($\alpha + \beta_1$) is represented by the point D while that corresponding to stable equilibrium ($\alpha + \beta_2$) is represented by the point E in the diagram. It has been validated experimentally that the metastable β_1 phase appears as the first precipitating phase during tempering of supersaturated α' (Zr–Nb) martensites avoiding the precipitation of the equilibrium β_2 phase [8, 9]. The precipitation of the metastable β_1 phase in preference to the equilibrium β_2 phase has also been experimentally demonstrated in another monotectoid system, Zr–Ta [10]. Preferential precipitation of the metastable β, being a characteristic of the Zr–Nb system, has a bearing on the microstructural changes during the creep process which will be discussed next.

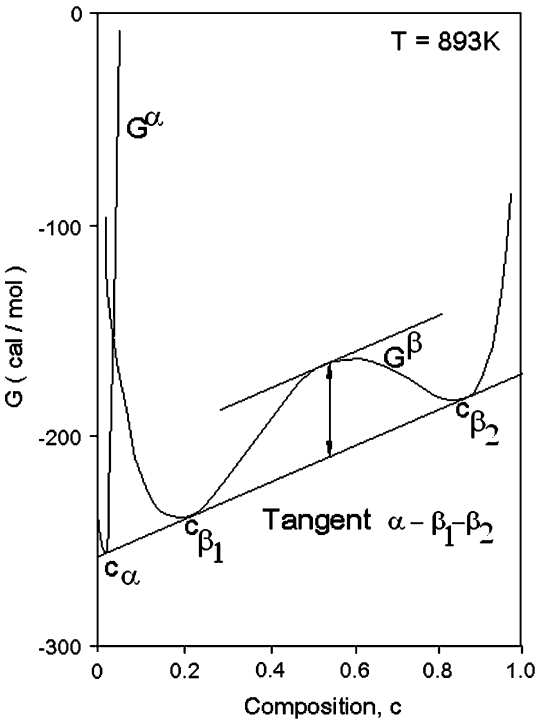

Fig. 7 Schematic free energy-composition diagram for Zr–Nb alloy system at 893 K

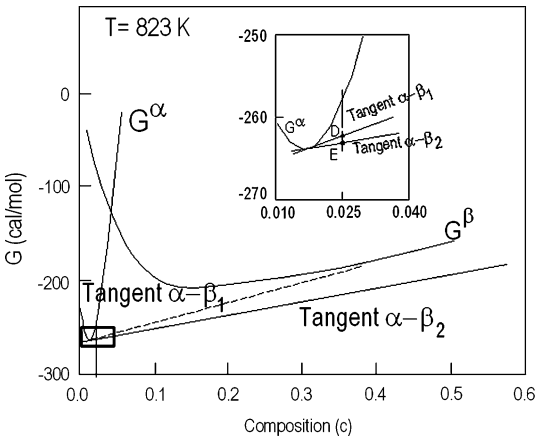

Fig. 8 Zr-rich portion of the Zr–Nb free energy composition diagram at 823 K indicating that the free energy of the ($\alpha + \beta_1$) mixture [7] is only slightly higher than that of the ($\alpha + \beta_2$) mixture. The ΔG difference is shown as D–E in the inset

Atomic volumes of β_1 and β_2

The stabilities of the three phases, α, β_1 and β_2, discussed in the previous paragraphs pertain to the situation corresponding to the absence of any external stress. It is also necessary to examine the stabilities of the three phases in the presence of externals stress. The observed lattice parameters [11, 12] of the α, β_1 and β_2 phases are as follows:

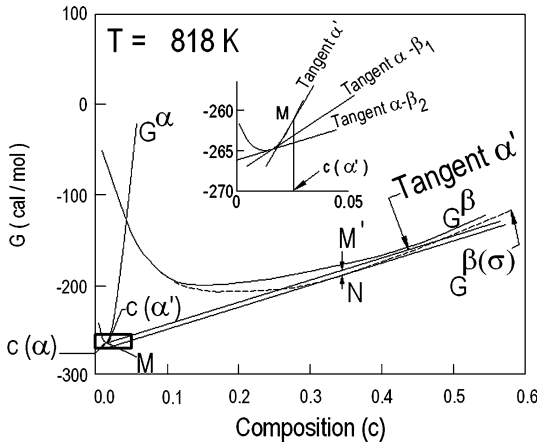

Fig. 9 The drop in the free energy of G^{β_1} arm of the G^{β}–c curve is because of external stress. The inset shows that the point M is the super-saturated composition of α ($c(\alpha')$) and the distance M′–N is the free energy difference between the super-saturated α phase and the location in the grain which experiences a tensile stress. The common tangent between α and β_1 at ~0.35 Nb indicates the equilibrium composition for β_1 for a stress of 4 MPa (see text)

$$a_\alpha = 0.3231\,\text{nm}, \quad c_\alpha = 0.5148\,\text{nm};$$
$$\beta_1 = 0.3540\,\text{nm}; \quad \text{and} \quad \beta_2 = 0.3350\,\text{nm}$$

With these lattice parameters, the volume per atom of the three phases Ω_α, Ω_{β_1}, and Ω_{β_2} will be as follows:

$$\Omega_\alpha = 23.270 \times 10^{-3}\,\text{nm}^3; \quad \Omega_{\beta_1} = 22.181 \times 10^{-3}\,\text{nm}^3$$
$$\text{and} \quad \Omega_{\beta_2} = 18.798 \times 10^{-3}\,\text{nm}^3$$

One can expect the external stress to influence the relative stabilities of β_1 and β_2 due to the difference in the volume per atom of the two phases. The presence of a tensile stress will favour the formation of β_1 in preference to β_2 as the volume per atom corresponding to the formation of the former is larger as compared to the latter. This change in the relative stability of the phases will result in a drop in the free energy values corresponding to the β_1 arm of the G^{β} plot as is shown in Fig. 9 by a dashed line and this drop can be linearly related to the applied stress as $\Delta G^{\beta_1} = \sigma_a \cdot (\Delta\Omega)$, where $\Delta\Omega = \frac{1}{3}\left(\Omega_{\beta_1} - \Omega_{\beta_2}\right)$. Substituting the maximum value of σ_a used in the present experiments, ΔG^{β_1} works out to be about 10 cals/mol and the ΔG^{β_1}–c curve under stress has been plotted accordingly (dashed curve in Fig. 9).

Likely mechanism

Keeping in view that the creep data at 818 K pointed to a stress exponent of unity suggestive of a diffusional creep process, it will be useful to attempt eliciting its underlying mechanism in the differently heat-treated samples.

Sample B

Diffusing Zr as well as Nb atoms are expected to move predominantly along the interfaces, grain boundaries and sub-boundaries. Dissolution of β_2 precipitates lying at those grain boundaries experiencing compressive stress and formation of β_1 precipitates at the grain boundaries experiencing tensile stress will become thermodynamically feasible if there is a net driving force for such a process. As the equilibrium ($\alpha + \beta_2$) and metastable ($\alpha + \beta_1$) phase mixtures have nearly the same free energy values (inset Fig. 8) and the fact that the application of stress lowers the β_1 arm of the G^{β}–c plot ($G^{\beta(\sigma)}$ dashed plot in Fig. 9), it is quite possible that the equilibrium shifts in favour of the $\alpha + \beta_1$ configuration. The tendency for preferential precipitation of β_1, also observed, as mentioned earlier, during the tempering of Zr–Nb martensite [8] appears to be further accentuated by the stress-aided shift in favour of $\alpha + \beta_1$ configuration.

Let us examine this process in detail with the help of the schematic in Fig. 10a and b. As a β_2 precipitate gradually dissolves in a region experiencing compressive stress (point X in Fig. 10), the local concentration of Nb atoms in the α phase around the region is raised and a concentration gradient of Nb is established between the point X and the point Y, where the latter is a location on the grain boundary experiencing tensile stress. The supersaturation of the α phase in niobium concentration, due to dissolution of the β_2 precipitates, can be represented in the G^{β}–c plot (inset in Fig. 9) by the point M corresponding to a Nb concentration of c (α'). Tangent α' is a line drawn as tangent to G^{α} curve at M. Considering the thermodynamics of the nucleation process [13], the drop in free energy for the nucleation will be maximum at a point N on the $G^{\beta(\sigma)}$–c plot where N is determined by a point where a line drawn parallel to tangent α' (MM′) touches the $G^{\beta(\sigma)}$ curve (Fig. 9). The vertical distance between the two lines, as shown by M′N in Fig. 9, indicates the drop in free energy associated with nucleation of the β phase. It may be noted that the Nb concentration of the re-precipitated β phase corresponds to about 0.35 which is consistent with the experimental observations (Table 4).

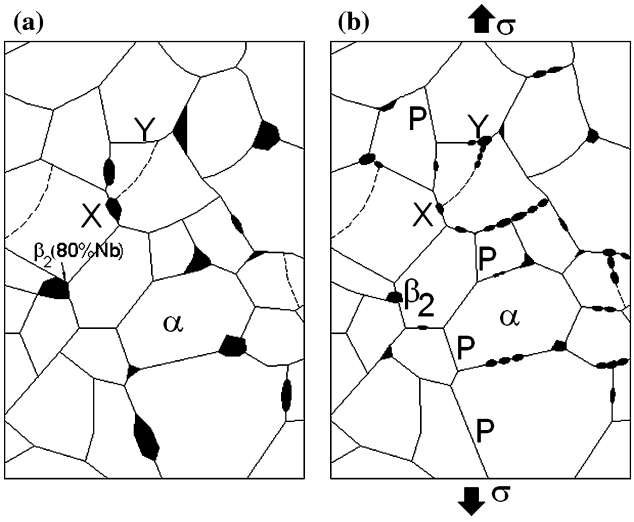

Fig. 10 Schematic showing the distribution of β phase before (**a**) and after (**b**) creep test, respectively. The dashed line X–Y marks a sub-boundary

Sample A

When we consider sample A which consists of α grains with β_1 precipitates at grain boundaries, the microstructural changes can be described in a similar manner. Also in this case, dissolution of β_1 particles enriches the Nb content of the α phase resulting in supersaturation in the proximity of the particles, following which nucleation of the β phase occurs at favourable sites. The arguments cited for sample B remain valid for the sample A as well in explaining the re-precipitation behaviour of the β phase.

In sample A the Nb content of the precipitate corresponding to maximum driving force for nucleation will be higher than 20%, the Nb concentration of the β_1 phase prior to creep deformation (sample A). Under the creep deformation condition, as long as atom movements from compressive stress regions to tensile stress regions continue, the re-precipitated β phase will maintain a composition indicated by the point N where the driving force for nucleation is maximum.

Based on the aforementioned thermodynamic argument, one can explain the observed changes in composition and volume fraction of the precipitate phase in both samples A (containing $\alpha + \beta_1$ phase mixture) and B (with $\alpha + \beta_2$ phase mixture) (Table 4). The re-precipitated β phases in the crept samples (both samples A and B) exhibit compositional distribution with a mean Nb concentration close to 0.35. In sample A, the Nb concentration of the re-precipitated β phase shifts towards a higher value, whereas that in sample B the shift is in the opposite direction. It is important to note (section "Atomic volumes of β_1 and β_2") that the atomic volume of β phase increases with decreasing Nb content $\left(\Omega_{\beta_1} > \Omega_{\beta_2}\right)$. Consequently, the transformation of $\alpha + \beta_2$ (80 wt.%Nb) to $\alpha + \beta$ ($\sim$35 wt.%) in sample B is expected to contribute additional strain ($\sim +2.30 \times 10^{-4}$) during creep deformation. This transformation strain could be significant due to a substantially lower Nb in the β-reprecipitate. In contrast, in sample A the re-precipitated β will have a higher Nb content ($\sim$35 wt.%) compared to β_1 (20 wt.% Nb) prior to creep. By the same argument based on atomic volumes, in sample A, the transformation $\alpha + \beta_1$ (20 wt.% Nb) to $\alpha + \beta$ (35 wt.% Nb) should be making a negative strain

contribution ($\sim -6.60 \times 10^{-4}$) and therefore to lowering the creep rate.

The measured changes in volume fraction and the observed creep rates in samples A and B are consistent with this interpretation. The phenomenon we have described may be summarized as follows:

The observed microstructural changes due to the creep process, and the fact that the equilibrium between $\alpha + \beta_1$ and $\alpha + \beta_2$ are closely competing, suggest that external stress can cause a change in the system from stable ($\alpha + \beta_2$) to metastable ($\alpha + \beta_1$).

In a diffusional creep situation, material flow is governed by a change in the chemical potential of components induced by stress. In the present case, an interplay of stress and phase stability operates during the creep process. Changes in volume fraction, in concentration and in morphology of the second phase, provide direct evidence of mass transfer from one grain facet to another. Trails of precipitates observed (Fig. 11) in the crept sample mark the path of the material flow.

It is evident from the foregoing that atom diffusion underlies the observed microstructural changes. Creep data can therefore be analyzed in terms of grain boundary or interface diffusion-controlled creep processes in order to identify the dominant flow process, as lattice diffusion-controlled creep processes are unlikely to contribute significantly to flow at 818 K, which is below $0.4T_m$, where T_m is the absolute melting temperature. The alternative is to consider grain boundary (or interface) diffusivity. Creep rates ($\dot{\varepsilon}_c$) are calculated using the flow relationship given by Eq. 2 assuming all the parameters to be the same except diffusivity. Diffusivity is to be taken as D_B for grain boundary diffusion-controlled creep and D_i for interface diffusion-controlled creep.

$$\dot{\varepsilon}_c = \frac{A_C \Omega w \sigma_{eff}}{d^3 kT} (D_B \text{ or } D_i) \quad (2)$$

In Eq. 2, A_C is a constant, Ω is the atomic volume, w is the grain boundary width and kT has the usual meaning. In Eq. 2, effective stress ($\sigma_a - \sigma_{th}$) is to be used to account for the observed threshold stress (Fig. 4b).

Measured creep rates are compared in Table 5 with those predicted by grain boundary diffusion-controlled creep and interface diffusion-controlled creep processes. Interface diffusivity, D_i (3.1×10^{-15} m^2/s), is markedly slower than grain boundary diffusivity, D_B (5.52×10^{-12} m^2/s), and so the interface diffusion can be regarded as rate controlling. It is evident from the data given in Table 5 that, for treatments A and C, the measured creep rates match well with those predicted by the interface diffusion-controlled creep mechanism but not with those for grain boundary diffusion creep. For the treatments A and C, creep rates calculated for grain boundary diffusion-controlled creep are nearly three orders of magnitude higher than the measured creep rates. This exercise points to interface diffusion-controlled creep as the likely operating mechanism.

Given that the β_2 or β_1 phases occur predominantly at interfaces and sub-boundaries, atom movement can be expected to be triggered at the precipitate–matrix (α phase) interface once the related activation barrier is overcome. Thereafter Zr or Nb diffusion could occur along the grain boundaries dictated by the chemical potential gradient set-up between the compressive and tensile facets, as remarked earlier. Interestingly, for treatment B, with interface diffusion-controlled creep as the operating mechanism, as suggested above, the measured creep rate is nearly an order of magnitude higher than the calculated value. Clearly,

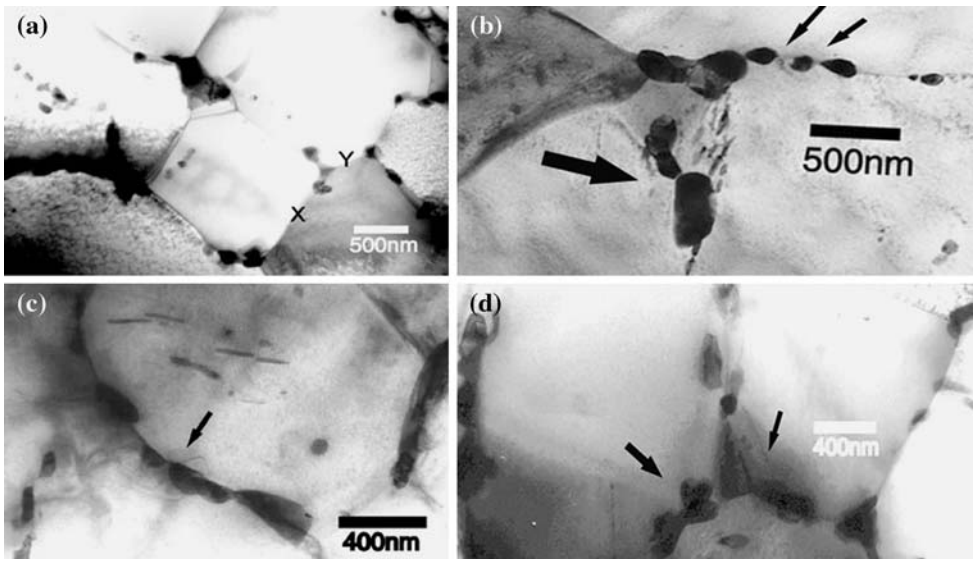

Fig. 11 TEMs showing evidence for reprecipitation of large size β_2 into smaller β phase ($\sim$30% Nb). (**a** & **b**) Finer precipitates can be seen as an array along the α-grain boundaries (*arrows*). (**c** & **d**) Also seen are trails of the diffusing species (Nb/Zr atoms) along intra-grain sub-boundaries (*arrows*) (helical sample)

Table 5 A comparison of measured creep rates with those predicted at 818 K (helical sample)

Treatment	Experimental conditions	Measured creep rate (s^{-1})	Calculated creep rate (s^{-1})		$\left(\frac{\text{Measured}}{\text{Calculated}}\right)$	
			Grain boundary controlled	Interface controlled	Grain boundary controlled	Interface controlled
A	$d = 3$ μm $\sigma_a = 2$ MPa	2.5×10^{-9}	5.9×10^{-6}	3.7×10^{-9}	4.2×10^{-4}	0.68
B	$d = 3$ μm $\sigma_a = 2$ MPa	1.8×10^{-7}	3.7×10^{-6}	2.3×10^{-9}	4.9×10^{-2}	78
C	$d = 5.1$ μm $\sigma_a = 4$ MPa	2.8×10^{-9}	1.6×10^{-6}	2.0×10^{-9}	1.8×10^{-3}	1.4

$w = 2b = 6.46 \times 10^{-10}$ m

$\Omega = 0.7b^3 = 2.36 \times 10^{-19}$ m^3

$D_{OB} = 7.5 \times 10^{-5}$ m^2/s and $Q_B = 111.7$ kJ/mol (taken from Knoor and Nortis [17]

$D_{Oi} = 8.4 \times 10^{3}$ m^2/s and $Q_i = 288$ kJ/mol (taken from Piotrkwoski and Dyment [18]

another phenomenon must be contributing to creep flow besides mass transport. We suggest that the transformation of $\alpha + \beta_2$ to $\alpha + \beta$ phase mixture, described earlier in this section, could be the additional contributor to creep flow. This is understandable since the positive volume change accompanying the reprecipitated β phase at tensile grain boundary facet is large enough to justify the enhanced creep rate.

It is relevant to point out that the variation of Nb content in the β phase observed after high-temperature creep deformation in the present work is analogous to that reported in pressure tubes of the same alloy irradiated in a nuclear reactor [14]. Griffiths et al. [14] have reported that the Nb contents in the β phase varied considerably (from 37% to 75%) in the Zr–2.5Nb pressure tubes after 2–14 years of service. The Nb content of the β phase has been found to attain a neutron flux and temperature-dependent steady state value after 2–3 years of operation. The net effect of temperature and neutron flux has been reported to be consistent with the nucleation of precipitate redistribution proposed by Nelson et al. [15] involving a balance between the rate of radiation-induced precipitate distribution and radiation-induced rate of growth.

Morphological features of β phases

Morphological features in sample B prior to and post-tensile creep deformation reveal the following:

(a) Prior to creep deformation, the β phase regions have been primarily distributed at the grain boundary tri-junctions and along grain boundaries (Fig. 6a, c). The tendency for minimization of the α/β interface area is reflected in the blocky appearance of the β phase regions. Such a distribution suggests that the annealing treatment (923 K/3 h) was adequate for complete recrystallization of the two phase structures. As a result of recrystallization and because the α/β interfacial energy is lower than that of the α/α interfacial energy, the minor β phase appears at grain boundaries and grain boundary tri-junction [16]. The special orientation relationship (Burgers type) between the β and α phases results in establishing geometric arrangements of interfacial dislocations along α/β interfaces [16].

(b) Subsequent to creep deformation, the β phase regions do not remain in the blocky form (Fig. 6b, d). The β phase regions appear distributed along the grain boundaries often in the form of a connected array of particles. In addition, trails of β particles are seen to be attached to massive β phase precipitates (marked as * in Fig. 6d) preferentially along a set of grain boundaries which are nearly parallel. Absence of precipitates in the grain boundaries which are perpendicular to the former (marked as 'P' in Fig. 6d) suggests the direction of externally applied stress, as schematically illustrated in Fig. 10b. These features are common observations at various locations in the specimens (Fig. 11a–d).

The observed changes in morphology and volume fraction of the β phase due to creep deformation point to creep flow resulting from a diffusive movement of atoms involving dissolution and re-precipitation of the β phase.

Conclusions

Studies of low-stress creep were conducted in a Zr–2.5%Nb alloy subjected to different heat treatments. Under the test conditions studied, stable and metastable second phases compete in the presence of an applied stress which influences their relative stabilities.

The creep deformation promotes the nucleation of a metastable phase and reduces the volume fraction of the stable phase. A stress level as small as 1–4 MPa is sufficient to cause this transformation by depressing the G^{β_1}–c arm of the free energy plot.

As a result of the above stress-induced transformation at elevated temperatures, the creep rate was observed to increase over an order of magnitude in the investigated stress range.

The changes in the morphology, composition and volume fraction of the β phase in the crept samples constitute evidence for stress-induced mass transfer and the formation of the metastable precipitates.

Acknowledgements One of us (P. Rama Rao) is grateful to the Indian Space Research Organization for the award of a Professorship. The authors place on record their grateful thanks to Dr. G. Malakondaiah of Defence Metallurgical Research Laboratory for his valuable suggestions and to Professor G.W. Greenwood of the University of Sheffield, UK for his helpful comments.

References

1. Masalski TB (Editor-in-Chief) (1992) Binary alloy phase diagrams, 2nd edn., vol 3. ASM International, Materials Park, p 2788
2. Prasad N, Malakondaiah G, Rama Rao P (1988) J Nucl Mater 158:30
3. Kaddour D, Frechinet S, Gourges AF, Brachet JC, Portier L, Pineau A (2004) Scr Mater 51:515
4. Malakondaiah G, Rama Rao P (1978) Trans Indian Inst Met 31:361
5. Towle DJ, Jones H (1976) Acta Metall 24:399
6. Malakondaiah G, Rama Rao P (1981) Acta Metall 29:1263
7. Menon SK, Banerjee S, Krishnan R (1978) Metall Trans A 9:1213
8. Banerjee S, Vijayakar SJ, Krishnan R (1976) J Nucl Mater 62:229
9. Luo CP, Weatherly GC (1987) Acta Metall 35:1963
10. Mukhopadhyay P, Menon ESK, Banerjee S, Krishnan R (1978) Z Metallkd 69:725
11. Pearson WB (1967) A handbook of lattice spacings and structures of metals and alloys. Pergamon Press, Oxford, p 79
12. Goldak J, Lloyd LT, Barret CS (1966) Phys Rev 144:478
13. Christian JK (1965) In: Raynor GV (ed) The theory of transformation in metals and alloys, vol 7. International series of monographs in metal physics and physical metallurgy. Pergamon Press, Oxford, p 606
14. Griffiths M, Mecke JF, Winegar JE (1996) In: Bradldy ER, Sabol GP (eds) Zirconium in the nuclear industry: eleventh international symposium, 11–14 September 1995, ASTM STP 1295. ASTM, West Conshohocken, p 580
15. Nelson RS, Hudson JA, Mazey D (1972) J Nucl Mater 44:318
16. Banerjee S, Dey GK, Srivastava D, Ranganathan S (1997) Metall Mater Trans A 28:2201
17. Knoor DG, Nortis MR (1975) J Nucl Mater 56:18
18. Piotrkwoski R, Dyment F (1991) J Nucl Mater 183:221